leads to a signal tuning range of 520 nm, between 1515 and 2040 nm, while the corresponding idler is tuned over 1340 nm, between 2220 and 3560 nm.

For an overview of OPO and OPA, the reader may refer to the following special issues of the *Journal of the Optical Society of America B*: (1993), **10**(9), 1656–1794; (1993), **10**(11), 2148–2239 and (1995), **12**(11), 2084–2310; and to the *Handbook of Optics* devoted to OPO (Ebrahimzadeh & Dunn, 2000).

1.7.4. Determination of basic nonlinear parameters

We review here the different methods that are used for the study of nonlinear crystals.

1.7.4.1. *Phase-matching directions and associated acceptance bandwidths*

The very early stage of crystal growth of a new material usually provides a powder with particle sizes less than 100 μm. It is then impossible to measure the phase-matching loci. Nevertheless, careful SHG experiments performed on high-quality crystalline material may indicate whether the SHG is phase-matched or not by considering the dependence of the SHG intensity on the following parameters: the angle between the detector and the direction of the incident fundamental beam, the powder layer thickness, the average particle size and the laser beam diameter (Kurtz & Perry, 1968). However, powder measurements are essentially used for the detection in a simple and quick way of noncentrosymmetry of crystals, this criterion being necessary to have a nonzero $\chi^{(2)}$ tensor (Kurtz & Dougherty, 1978). They also allow, for example, the measurement of the temperature of a possible centrosymmetric/noncentrosymmetric transition (Marnier *et al.*, 1989).

For crystal sizes greater than few hundred μm, it is possible to perform direct measurements of phase-matching directions. The methods developed at present are based on the use of a single crystal ground into an ellipsoidal (Velsko, 1989) or spherical shape (Marnier & Boulanger, 1989; Boulanger, 1989; Boulanger *et al.*, 1998); a sphere is difficult to obtain for sample diameters less than 2 mm, but it is the best geometry for large numbers and accurate measurements because of normal refraction for every chosen direction of propagation. The sample is oriented using X-rays, placed at the centre of an Euler circle and illuminated with fixed and appropriately focused laser beams. The experiments are usually performed with SHG of different fundamental wavelengths. The sample is rotated in order to propagate the fundamental beam in different directions: a phase-matching direction is then detected when the SHG conversion efficiency is a maximum. It is then possible to describe the whole phase-matching cone with an accuracy of 1°. A spherical crystal also allows easy measurement of the walk-off angle of each of the waves (Boulanger *et al.*, 1998). It is also possible to perform a precise observation and study of the internal conical refraction in biaxial crystals, which leads to the determination of the optic axis angle $V(\omega)$, given by relation (1.7.3.14), for different frequencies (Fève *et al.*, 1994).

Phase-matching relations are often poorly calculated when using refractive indices determined by the prism method or by measurement of the critical angle of total reflection. Indeed, all the refractive indices concerned have to be measured with an accuracy of 10^{-4} in order to calculate the phase-matching angles with a precision of about 1°. Such accuracies can be reached in the visible spectrum, but it is more difficult for infrared wavelengths. Furthermore, it is difficult to cut a prism of few mm size with plane faces.

If the refractive indices are known with the required accuracy at several wavelengths well distributed across the transparency region, it is possible to fit the data with a Sellmeier equation of the following type, for example:

$$n_i^2(\lambda) = A_i + \frac{B_i\lambda^2}{\lambda^2 - C_i} + D_i\lambda^2. \qquad (1.7.4.1)$$

n_i is the principal refractive index, where $i = o$ (ordinary) and e (extraordinary) for uniaxial crystals and $i = x$, y and z for biaxial crystals.

It is then easy to calculate the phase-matching angles (θ_{PM}, φ_{PM}) from (1.7.4.1) using equations (1.7.3.27) or (1.7.3.29) where the angular variation of the refractive indices is given by equation (1.7.3.6).

The measurement of the variation of intensity of the generated beam as a function of the angle of incidence can be performed on a sphere or slab, leading, respectively, to internal and external angular acceptances. The thermal acceptance is usually measured on a slab which is heated or cooled during the frequency conversion process. The spectral acceptance is not often measured, but essentially calculated from Sellmeier equations (1.7.4.1) and the expansion of Δk in the Taylor series (1.7.3.43) with $\xi = \lambda$.

1.7.4.2. *Nonlinear coefficients*

The knowledge of the absolute magnitude and of the relative sign of the independent elements of the tensors $\chi^{(2)}$ and $\chi^{(3)}$ is of prime importance not only for the qualification of a new crystal, but also for the fundamental engineering of nonlinear optical materials in connection with microscopic aspects.

However, disparities in the published values of the nonlinear coefficients of the same crystal exist, even if it is a well known material that has been used for a long time in efficient devices (Eckardt & Byer, 1991; Boulanger, Fève *et al.*, 1994). The disagreement between the different absolute magnitudes is sometimes a result of variation in the quality of the crystals, but mainly arises from differences in the measurement techniques. Furthermore, a considerable amount of confusion exists as a consequence of the difference between the conventions taken for the relation between the induced nonlinear polarization and the nonlinear susceptibility, as explained in Section 1.7.2.1.4.

Accurate measurements require mm-size crystals with high optical quality of both surface and bulk.

1.7.4.2.1. *Non-phase-matched interaction method*

The main techniques used are based on non-phase-matched SHG and THG performed in several samples cut in different directions. The classical method, termed the Maker-fringes technique (Jerphagnon & Kurtz, 1970; Herman & Hayden, 1995), consists of the measurement of the harmonic power as a function of the angle between the fundamental laser beam and the rotated slab sample, as shown in Fig. 1.7.4.1(*a*).

The conversion efficiency is weak because the interaction is non-phase-matched. In normal incidence, the waves are collinear and so formulae (1.7.3.42) for SHG and (1.7.3.80) for THG are valid. These can be written in a more convenient form where the coherence length appears:

$$\begin{aligned} P^{n\omega}(L) &= A^{n\omega}[P^{\omega}(0)]^n (d_{\rm eff}^{n\omega} \cdot l_c^{n\omega})^2 \sin^2(\pi L/2l_c^{n\omega}) \\ l_c^{2\omega} &= (\pi c/\omega)(2n_3^{2\omega} - n_1^{\omega} - n_2^{\omega})^{-1} \\ l_c^{3\omega} &= (\pi c/\omega)(3n_4^{3\omega} - n_1^{\omega} - n_2^{\omega} - n_3^{\omega})^{-1}. \end{aligned} \qquad (1.7.4.2)$$

The coefficient $A^{n\omega}$ depends on the refractive indices in the direction of propagation and on the fundamental beam geometry: $A^{2\omega}$ and $A^{3\omega}$ can be easily expressed by identifying (1.7.4.2) with (1.7.3.42) and (1.7.3.80), respectively.

When the crystal is rotated, the harmonic and fundamental waves are refracted with different angles, which leads to a variation of the coherence length and consequently to an oscillation of the harmonic power as a function of the angle of incidence, α, of the fundamental beam. Note that the oscillation

Table 1.7.5.1. *Mineral nonlinear crystals*

The letters (*a*, *b*, *c*) refer to the crystallographic frame. These data are mainly extracted from Bordui & Fejer (1993).

(*a*) SHG (1.064–0.532 μm).

	KD_2PO_4 (KD*P)	$NH_4H_2PO_4$ (ADP)	CsD_2AsO_4 (CD*A)	β-BaB_2O_4 (BBO)	LiB_3O_5 (LBO)
Crystal class	$\bar{4}2m$	$\bar{4}2m$	$\bar{4}2m$	$3m$	$mm2$
Transparency (μm)	0.18–1.8	0.184–1.5	0.27–1.66	0.198–2.6	0.16–2.3
Non-critical λ_{pump} at room temperature (μm)					
Type I	0.519	0.524	1.045	0.409	0.554 (*c*) 1.212 (*a*)
Type II	—	—	—	—	1.19 (*b*)
T_{pm} (K)			385		421
Type of phase matching	II	II	I	I	I (*a*)
θ (°)	54	62	90	23	90
φ (°)	—	—	—	—	0
Effective coefficient d_{eff} (pm V^{-1})	0.35	0.39	0.30	1.9	0.85
Angular bandwidth (mrad cm)	2.3	2.2	51	0.53	72
Walk-off angles					
ρ^{ω} (°)	1.3	1.2	0	0	0
$\rho^{2\omega}$ (°)	1.4	1.5	0	3.2	0
Thermal bandwidth (K cm)	12	2.1	3.3	51	3.9
Spectral bandwidth (nm cm)	5.6	26	2.5	2	3.6
Surface optical damage threshold (GW cm^{-2})	5 (1 ns) >8 (0.6 ns at 0.53 μm)	6 (15 ns) >8 (0.6 ns at 0.53 μm)	0.25 (12 ns)	13.5 (1 ns) 23 (14 ns) 32 (8 ns at 0.53 μm)	25 (0.1 ns) 1.4 (12 ns at 0.78 μm)

SHG (1.064–0.532 μm) (*cont.*).

	$KTiOPO_4$ (KTP)	$KNbO_3$	5% MgO:$LiNbO_3$	$LiIO_3$
Crystal class	$mm2$	$mm2$	$3m$	$6mm$
Transparency (μm)	0.35–4.5	0.4–5.5	0.35–5	0.31–5 || to **c**, 0.34–4 ⊥ to **c**
Non-critical λ_{pump} at room temperature (μm)				
Type I	—	0.860 (*a*) 0.982 (*b*)		0.756
Type II	0.990 (*b*) 1.081 (*a*)	—		—
T_{pm} (K)		456	380	
Type of phase matching	II (*a*, *b*)	I (*b*)	I	I
θ (°)	90	90	90	30
φ (°)	23	90	—	—
Effective coefficient d_{eff} (pm V^{-1})	2.4	−13	4.7	1.8
Angular bandwidth (mrad cm)	9	13	33	0.34
Walk-off angles				
ρ^{ω} (°)	0.20	0	0	0
$\rho^{2\omega}$ (°)	0.27	0	0	4.3
Thermal bandwidth (K cm)	17	0.3	0.75	23
Spectral bandwidth (nm cm)	0.46	0.12	0.31	0.82
Surface optical damage threshold (GW cm^{-2})	9–20 (1 ns) >2 (10 ns at 0.5 μm)	7 (1 ns) >1 (10 ns)		2 (1 ns) 1 (0.1 ns at 0.53 μm)

(*b*) SHG (532–266 nm).

	KD_2PO_4 (KD*P)	$NH_4H_2PO_4$ (ADP)	β-BaB_2O_4 (BBO)
Crystal class	$\bar{4}2m$	$\bar{4}2m$	$\bar{4}2m$
Transparency (μm)	0.18–1.8	0.184–1.5	0.198–2.6
Non-critical λ_{pump} at room temperature (μm)	0.519	0.524	0.409
T_{pm} (K)	308	324	
Type of phase matching	I	I	I
θ (°)	90	90	47
φ (°)	—	—	—
Effective coefficient d_{eff} (pm V^{-1})	0.44	0.57	2.0
Angular bandwidth (mrad cm)	16	16	0.16
Walk-off angles			
ρ^{ω} (°)	0	0	0
$\rho^{2\omega}$ (°)	0	0	4.8
Thermal bandwidth (K cm)	3.0	0.54	4.0
Spectral bandwidth (nm cm)	0.13	0.13	0.073
Surface optical damage threshold (GW cm^{-2})	5 (1 ns) >8 (0.6 ns at 0.53 μm)	6 (15 ns) >8 (0.6 ns at 0.53 μm)	13.5 (1 ns) 23 (14 ns) 32 (8 ns at 0.53 μm)

Table 1.7.5.1 (*cont.*)

(*c*) SHG (4000–2000 nm).

	$AgGaS_2$	$AgGaSe_2$	$ZnGeP_2$	Tl_3AsSe_3 (TAS)
Crystal class	$\bar{4}2m$	$\bar{4}2m$	$\bar{4}2m$	$3m$
Transparency (μm)	0.5–13	0.78–18	0.74–12	1.3–17
Non-critical λ_{pump} at room temperature (μm)	1.8 and 11.2	3.1 12.8	3.2 10.3	—
Type of phase matching	I	I	I	I
θ (°)	31	52	56	33
φ (°)	—	—	—	—
Effective coefficient d_{eff} (pm V^{-1})	10.4	28	70	68
Angular bandwidth (mrad cm)	3.7	6.0	5.0	4.2
Walk-off angles				
ρ^{ω} (°)	0	0	0.65	0
$\rho^{2\omega}$ (°)	1.2	0.64	0	3.1
Thermal bandwidth (K cm)	50	50	40	5.7 (SHG at 10.6 μm)
Spectral bandwidth (nm cm)	11	22	20	—
Surface optical damage threshold (GW cm^{-2})	0.5 (10 ns bulk)	0.01–0.04 (50 ns, 2 μm) 0.02–0.03 (10 ns at 10.6 μm)	0.05 (25 ns at 2 μm) 1 (2 ns at 10.6 μm)	0.016 (250 ns at 10.6 μm)

exists even if the refractive indices do not vary with the direction of propagation, which would be the case for an interaction involving only ordinary waves during the rotation. The most general expression of the generated harmonic power, *i.e.* $P^{n\omega}(\alpha) = j(\alpha)\sin^2\Psi(\alpha)$, must take into account the angular dependence of all the refractive indices, in particular for the calculation of the coherence length and transmission coefficients (Herman & Hayden, 1995). The effective coefficient is then deduced from the angular spacing of the Maker fringes and from the conversion efficiency at the maxima of oscillation.

A continuous variation of the phase mismatch can also be performed by translating a wedged sample as shown in Fig. 1.7.4.1(*b*) (Perry, 1991). The harmonic power oscillates as a function of the displacement x. In this case, the interacting waves stay collinear and the oscillation is only caused by the variation of the crystal length. Relation (1.7.4.2) is then valid, by considering a variable crystal length $L(x) = x\tan\beta$; $A^{n\omega}$ and $l_c^{n\omega}$ are constant. The space between two maxima of the wedge fringes is $\Delta x_c = 2l_c/\tan\beta$, which allows the determination of l_c. Then the measurement of the harmonic power, $P_{max}^{n\omega}$, generated at a maximum leads to the absolute value of the effective coefficient:

$$|d_{eff}^{n\omega}| = \left\{\frac{P_{max}^{n\omega}}{A^{n\omega}[P^{\omega}(0)]^2 l_c^2}\right\}^{1/2}$$
$$l_c = (\Delta x_c \tan\beta/2). \qquad (1.7.4.3)$$

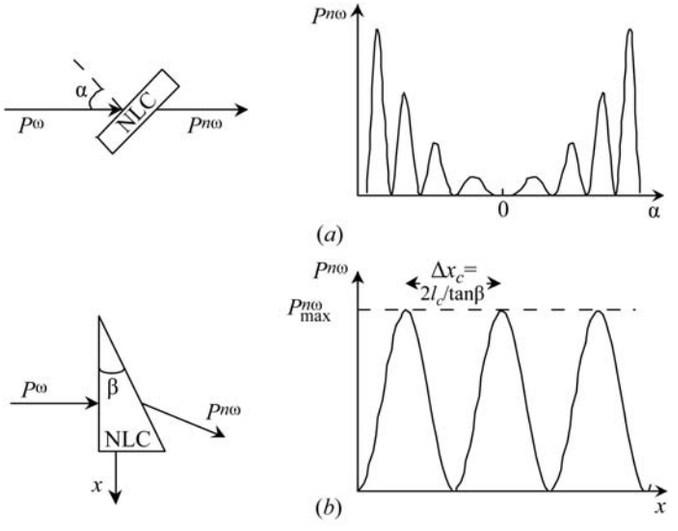

Fig. 1.7.4.1. (*a*) The Maker-fringes technique; (*b*) the wedge-fringes technique.

It is necessary to take into account a multiple reflection factor in the expression of $A^{n\omega}$.

The Maker-fringes and wedge-fringes techniques are essentially used for relative measurements referenced to a standard, usually KH_2PO_4 (KDP) or quartz (α-SiO_2).

1.7.4.2.2. *Phase-matched interaction method*

The use of phase-matched interactions is suitable for absolute and accurate measurements (Eckardt & Byer, 1991; Boulanger, Fève *et al.*, 1994). The sample studied is usually a slab cut in a phase-matching direction. The effective coefficient is determined from the measurement of the conversion efficiency using the theoretical expressions given by (1.7.3.30) and (1.7.3.42) for SHG, and by (1.7.3.80) for THG, according to the validity of the corresponding approximations. Because of phase matching, the generated harmonic power is not weak and it is measurable with very good accuracy, even with a c.w. conversion efficiency.

Recent experiments have been performed in a KTP crystal cut as a sphere (Boulanger *et al.*, 1997, 1998): the absolute magnitudes of the quadratic effective coefficients are measured with an accuracy of 10%, which is comparable with typical experiments on a slab.

For both non-phase-matched and phase-matched techniques, it is important to know the refractive indices and to characterize the spatial, temporal and spectral properties of the pump beam carefully. The considerations developed in Section 1.7.3 about effective coefficients and field tensors allow judicious choices of configurations of polarization and directions of propagation for the determination of the absolute value and relative sign of the independent coefficients of tensors $\chi^{(2)}$ and $\chi^{(3)}$, given in Tables 1.7.2.2 to 1.7.2.5 for the different crystal point groups.

1.7.5. The main nonlinear crystals

Tables 1.7.5.1 and 1.7.5.2 give some characteristics of the main nonlinear crystals. No single nonlinear crystal is the best for all applications, so the different materials must be seen as complementary to each other.

A complete review of mineral crystals is given in Bordui & Fejer (1993). General references for organic crystals may be found, for example, in Chemla & Zyss (1987), Zyss (1994), and Dmitriev *et al.* (1991). Perry (1991) deals with both organic and inorganic materials.

A new generation of materials has been developed since 1995 for the design of new compact all-solid-state laser sources. These optical materials are multifunction crystals, such as $LiNbO_3$:Nd^{3+}, $Ba_2NaNb_5O_{15}$:Nd^{3+}, $CaGd_4(BO_3)_3O$:Nd^{3+} or $YAl_3(BO_3)_4$:Yb^{3+}, for example, in which the laser effect and the nonlinear frequency